International Journal of Medical, Medicine and Health Sciences
ISSN: 2517-9969
Vol:4, No:5, 2010

Computer Models of the Vestibular Head Tilt Response, and their relationship to EVestG and Meniere's Disease

Daniel Heibert, Brian Lithgow, and Kerry Hourigan

***Abstract*—**This paper attempts to explain response components of Electrovestibulography (EVestG) using a computer simulation of a three-canal model of the vestibular system. EVestG is a potentially new diagnostic method for Meniere's disease. EVestG is a variant of Electrocochleography (ECOG), which has been used as a standard method for diagnosing Meniere's disease - it can be used to measure the SP/AP ratio, where an SP/AP ratio greater than 0.4-0.5 is indicative of Meniere's Disease. In EVestG, an applied head tilt replaces the acoustic stimulus of ECOG. The EVestG output is also an SP/AP type plot, where SP is the summing potential, and AP is the action potential amplitude. AP is thought of as being proportional to the size of a population of afferents in an excitatory neural firing state.

A simulation of the fluid volume displacement in the vestibular labyrinth in response to various types of head tilts (ipsilateral, backwards and horizontal rotation) was performed, and a simple neural model based on these simulations developed.

The simple neural model shows that the change in firing rate of the utricle is much larger in magnitude than the change in firing rates of all three semi-circular canals following a head tilt (except in a horizontal rotation). The data suggests that the change in utricular firing rate is a minimum 2-3 orders of magnitude larger than changes in firing rates of the canals during ipsilateral/backward tilts. Based on these results, the neural response recorded by the electrode in our EVestG recordings is expected to be dominated by the utricle in ipsilateral/backward tilts (It is important to note that the effect of the saccule and efferent signals were not taken into account in this model).

If the utricle response dominates the EVestG recordings as the modeling results suggest, then EVestG has the potential to diagnose utricular hair cell damage due to a viral infection (which has been cited as one possible cause of Meniere's Disease).

***Keywords*—**Diagnostic, Endolymph Hydrops, Meniere's Disease, Modeling.

I. Introduction

ONE of the main aims of this study was to find a relationship between Electrovestibulography (EVestG), which is a potentially new diagnostic method for Meniere's Disease, and computer simulations of a three-canal model of the vestibular system. The computer simulations are based on a mathematical model derived by Rabbitt, Damiano and Grant [1], a macro-mechanical model of all three semi-circular canals and utricle connected together. It was hoped that this model could be used to develop a simple computer simulation of the neural response of the vestibular system, which would then help explain certain aspects of the EVestG neural recording.

EVestG is a new technique being applied to measuring Meniere's Disease, and is purported to be able to record a direct vestibular response to an applied head tilt, unlike normal Electrocochleography (ECOG), which has its result derived from an acoustic response. Electrocochleography (ECOG) has been a standard method for diagnosing Meniere's disease for many years, and a large amount of literature exists on the subject [4], [6]. It can be used to measure the SP/AP ratio. The SP/AP ratio is used to diagnose Meniere's disease, and in particular, hydrops [6], where SP stands for summing potential, AP stands for action potential amplitude, and TAP is time of action potentials (see Fig. 1). The ECOG output is typically the SP/AP plot (Fig. 1) in which an SP/AP ratio greater than 0.4-0.5 is indicative of Meniere's Disease [4]. Similarly, the EVestG output is also an SP/AP type plot.

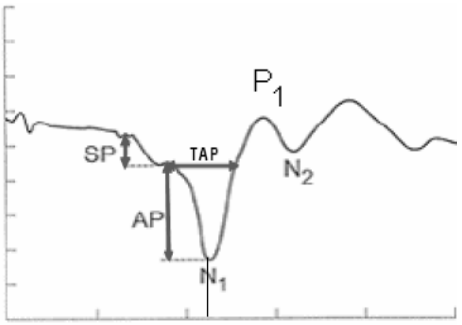

Fig. 1 Sp/Ap ratio and TAP definitions

Diagnosis of Meniere 's disease is made more difficult when patients are not suffering from acute symptoms. Misdiagnosis remains a problem [8]. As an example, [10] states, "Of those with definite Meniere's disease, (only) 66.7% had abnormally elevated SP/AP ratios". These limitations provide motivation to search for new, alternative diagnostic methods, such as EVestG. EVestG has also the potential to have many other diagnostic applications, particularly in the area of Parkinson's disease, as shown by other studies [13].

Daniel Heibert is with the Monash University Centre for Biomedical Engineering, Department of Electrical and Computing Systems Engineering, Monash University 3800, Australia

Brian Lithgow is with the Alfred Psychiatry Research Centre, Alfred Hospital, Prahan, Victoria, Australia (corresponding author to provide phone: +61 99051893; e-mail: Brian.Lithgow@eng.monash.edu.au).

Kerry Hourigan is with the Division of Biological Engineering, Monash University 3800, Australia

EVestG recordings are performed by tilting a patient in a computer controlled tilt chair, and placing an electrode close to the patient's tympanic membrane (eardrum) to record their vestibular neural response [14]. For this reason, it is particularly important to make a computer simulation of a *three-canal model* of the vestibular system, as a recording electrode in a subject's ear canal will record neural signals from each part of the vestibular labyrinth. Therefore, a three-canal model has the potential to explain the neural signal recorded.

The vestibular labyrinth is made up of three semi-circular canals: the anterior canal, posterior canal and horizontal (lateral) canal, which detect angular accelerations in three-dimensional space. Another important segment of the vestibular labyrinth is the utricle, which contains the utricular macula, an organ that detects *linear* acceleration mainly in the earth horizontal plane, and gravity when the head is not in its usual upright position (such as when the head is tilted sideways or backwards/forwards relative to the earth horizontal)[12]. The utricle is a membranous sac containing the *otolith membrane* [15]. The otolith membrane is essentially made up crystals (the otolith layer) embedded in a gelatinous mass that also contains hair cells. Because of the inertia of the crystals, when the human head undergoes ***linear*** acceleration they get "left behind", thus bending the hair cells with it. If the displacement of the otolith membrane (at a certain point) is in the direction of the hair cell's ***polarization vector***, maximum excitatory neural firing (due to the hair cells) occurs. The surface of the utricular macula has a complex pattern of polarization vectors, giving the utricular macula directional sensitivity [7].

The three-canal model by Rabbitt, Damiano and Grant [1] is suitable for modeling the vestibular labyrinth, as it is a simple macro-mechanical model that can be used to compute fluid volume displacements in each part of the labyrinth. Work by Obrist [17] has shown that the fluid dynamics of the semicircular canal translates the rotational velocity directly into a volume displacement of the cupula, and a subset of regularly discharging semicircular canal afferents directly reflect cupula volume displacement and encode angular velocity over a wide range of frequencies [16]. As a result, the fluid volume displacements in the semi-circular canals can be thought of as proportional to the neural response. A simple model of the utricular macula neural response was also developed, using a simple biomechanical model [1]. It was combined with an experimentally derived directional sensitivity map of the utricular macula [7].

Another central aim of this research was to vary the most relevant model parameters, to see how *stable* the solutions of equations of fluid flow in the three-canal model are. Considering that quite a few estimates were used in creating the simulation, testing the model to see how sensitive it is to errors is a very important part of this research.

One main limitation of the modeling work presented is that it does not include the *saccule,* which contains the saccular macula – an organ that senses linear acceleration mainly in the vertical plane. There is very limited fluid flow through the saccule during rotations, so it can be assumed that fluid flow does not affect the saccular macula [12]. However, the EVestG recordings may still detect neural activity of the saccule, particularly during a backwards/forwards tilt where the vertical component of gravity acting on the saccular macula changes. The three-canal model presented in this research focuses purely on the response of the semi-circular canals and utricular macula, which means that responses of the saccule will not be taken into account in the simulations.

EVestG is a new technique being applied to measuring Meniere's Disease and has the advantages that 1. it is purported to be able to record a direct vestibular response to an applied tilt that is recordable, unlike normal Electrocochleography (ECOG), even with hearing impaired subjects [18] and 2. its response plot width is reported [14] to be reflective of changes in response time constants.

As mentioned before, EVestG recordings are performed by tilting a patient in a computer controlled tilt chair, and placing an electrode close to the patient's eardrum to record their vestibular neural response [14]. The electrodes used are single-use electrodes, simply and painlessly positioned and resting on the left, right or both ear drums of the test subject. The neural response is divided into time segments (background, onset, onset + transient, transient, steady state). These time segments will be defined in the EVestG recording methods section. The EVestG-evoked response field potentials were extracted using a Neural Event Extraction Routine [20], [22] and these were averaged to produce an SP/AP-like plot for each time segment (refer to Fig. 1).

From these experiments, a sample of EVestG recordings of 11 Meniere's patients, and equally as many age matched controls, was used in this research.

That head tilt can be in a direction excitatory to the semicircular canals (ipsilateral side tilt) or more inhibitory (contralateral side tilt). The utricle is expected to have an overall excitatory neural response to head tilts in any direction [7]. Alternatively, the individual acceleration, deceleration and background phases of each tilt can be considered separately to obtain a performance index for each phase (a background recording is only possible with the new technique, EVestG). Therefore, an EVestG is likely more of a direct recording of the vestibular response, unlike the ECOG result that is derived from an acoustic response.

In the computer simulations of the vestibular head tilt response using the three-canal model [1], details of the EVestG laboratory set-up were taken into account. The tilt chair can rotate a patient horizontally, ipsilaterally/contralaterally (sideways), backwards/forwards. The rotation velocities are half cycle sinusoids. The chair can also move a patient up and down [14].

The main biomarkers of the EVestG plot will be explained in the methods and results sections. Second, how they can relate to the computer simulations of the vestibular head tilt response will be discussed.

II. Theoretical Background

A. Three Canal Model

The Rabbitt, Damiano and Grant [1] model connects the three semi-circular canals as shown in Fig. 2. The directions of volume fluid displacement, Q_{HC}, Q_{UP}, Q_{UA}, Q_{AC}, Q_{CC}, and Q_{PC} are shown corresponding to segments *HC* (horizontal slender canal segment), *UP* (posterior section of the utricle), *UA* (anterior section of the utricle), *AC* (anterior slender canal segment), *CC* (common crux section), and *PC* (posterior slender canal segment), respectively. The fluid inside the canals is assumed to be Newtonian and incompressible [1]. This is considered to be an excellent assumption in regards to endolymph [1], [12].

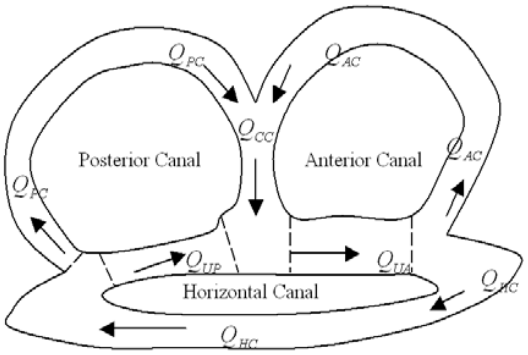

Fig. 2 The three-canal model, showing the direction of volume fluid displacement for each segment

The three-canal model is represented by a system of differential equations given by

$$[M]\frac{d^2\vec{Q}}{dt^2}+[C]\frac{d\vec{Q}}{dt}+[K]\vec{Q}=\vec{F}\,, \tag{1}$$

where

$$\vec{Q}=\begin{pmatrix} Q_{HC} \\ Q_{AC} \\ Q_{PC} \end{pmatrix}, \tag{2}$$

$$[M]=\begin{pmatrix} M_{HC} & -m_{UA} & +m_{UP} \\ -m_{UA} & M_{AC} & -m_{CC} \\ +m_{UP} & -m_{CC} & M_{PC} \end{pmatrix}, \tag{3}$$

$$[K]=\begin{pmatrix} K_{HC} & -k_{UA} & +k_{UP} \\ -k_{UA} & K_{AC} & -k_{CC} \\ +k_{UP} & -k_{CC} & K_{PC} \end{pmatrix}, \tag{4}$$

$$[C]=\begin{pmatrix} C_{HC} & -c_{UA} & +c_{UP} \\ -c_{UA} & C_{AC} & -c_{CC} \\ +c_{UP} & -c_{CC} & C_{PC} \end{pmatrix}, \tag{5}$$

and $\vec{F}=\begin{pmatrix} -f_{HC}-f_{UA}-f_{UP} \\ -f_{AC}-f_{CC}-f_{UA} \\ -f_{PC}-f_{CC}+f_{UP} \end{pmatrix}$. (6)

The six elements of the [M] (mass), [C] (damping) and [K] (stiffness) matrices are given by

$$m_n=\int_0^{l_n}\frac{\rho}{A}ds\,, \tag{7}$$

$$c_n=\int_0^{l_n}\frac{\mu\lambda_\mu}{A^2}ds\,, \tag{8}$$

$$k_n=\int_0^{l_n}\frac{\gamma\lambda_\gamma}{A^2}ds\,, \tag{9}$$

where l_n is the length of the particular segment *n*, ρ is the density of the endolymphatic fluid in the canals (g/cm^3), *s* is the distance along a particular segment *n*, *A(s)* is the local cross-sectional area of the rigid canal walls (cm^2) (Damiano [9], the stiffness of the endolymphatic duct was $Ed = 3.0\times10^3 dyne$,so we can assume the duct walls to be rigid), μ is the dynamic viscosity of the endolymph $(dyne.\sec ond/cm^2)$, γ is the cupular shear stiffness ($dyne/cm^2$), λ_μ is the dimensionless frequency dependent velocity profile, and λ_γ is a dimensionless displacement profile factor.

The elements M_n, C_n, and K_n (in the mass, damping and stiffness matrices) are given by (7), (8) and (9), respectively, except that the integrals are made to be closed contour integrals (over the length of each of the three semicircular canal loops).

The forcing vector elements (6) are given by

$$f_n=\ddot{\Omega}\,g_n\,, \tag{10}$$

where

$$g_n=\int_0^{l_n}\rho\vec{m}\times\vec{R}(s)\bullet\vec{ds}\,. \tag{11}$$

The vector $\vec{m}$ is the unit vector in the direction of the angular acceleration, $\ddot{\Omega}$ is the magnitude of the angular acceleration applied to the canals (rad/sec^2), $\vec{R}(s)$ is a vector pointing to the centerline of a canal, and $\vec{ds}$ is a vector tangent to the centerline of a canal. The pivot point (about which rotation occurs) is at the origin of the vector coordinate system.

By conservation of mass,

$$Q_{HC}-Q_{PC}=Q_{UP}\,, \tag{12}$$

$$Q_{AC} + Q_{PC} = Q_{CC}, \quad (13)$$

and

$$Q_{AC} + Q_{HC} = Q_{UA}. \quad (14)$$

The authors of this paper redid the algebra to obtain (1), and found that there was an **error** in the Springer text [1]. In order to maintain conservation of mass (as is assumed in this model), the coefficient of all matrix elements with subscript *UP* must be +1 (not –1, as in the Springer text). This correction is shown in (3)-(5).

The 'gross' or 'average' displacement of the otoconia layer (which causes hair cells to be bent on the utricular macula) in an arbitrary direction, $\hat{n}$ (in the plane of the utricle), is given by the transfer function for a step input acceleration [1]

$$T_0(\tilde{s}) = \frac{\tilde{u}}{\tilde{a}} = \frac{g_0/m_0}{(\tilde{s}+1/\tau_1)(\tilde{s}+1/\tau_2)}, \quad (15)$$

where $\tilde{u}(\tilde{s})$ is the gross displacement of the otoconia layer in the $\hat{n}$ direction, and $\tilde{a}(\tilde{s})$ is the gravitoinertial linear acceleration in the $\hat{n}$ direction, both expressed in the Laplace domain. In the time domain, $\tilde{a}(\tilde{s})$ is expressed as

$$a(t) = \hat{n} \bullet (\vec{g} - \ddot{\vec{X}}), \quad (16)$$

where $\vec{g}$ is the gravity vector, and $\ddot{\vec{X}}$ is the linear acceleration of the temporal bone (that the utricular macula is attached to). The displacement of the otoconia layer as a function of time, *u(t)*, is relative to the moving substrate i.e. the temporal bone. The time constants of the system are τ_1 and τ_2; g_0 and m_0 are known constants.

In the case of purely rotational (or angular) movements, the acceleration of the fluid through the utricle can be thought of as 'linear acceleration', and $\ddot{\vec{X}}$ is set to

$$\left|\ddot{\vec{X}}\right| = \frac{1}{A_{UA}} \frac{d^2 Q_{UA}}{dt^2}, \quad (17)$$

where A_{UA} is the average cross-sectional area of the utricle, and Q_{UA} is the fluid volume displacement in the utricle for a given rotation (ipsilateral/contralateral, backwards or horizontal rotations).

B. Meniere's Disease

Meniere's disease is a pathology of the vestibular system, and its symptoms include fluctuating hearing loss, tinnitus, episodic vertigo and a sensation of fullness or pressure in the ear [15]. It appears that the main pathology in Meniere's syndrome is an increase in the volume and pressure of endolymph, which can cause a distention of the endolymphatic system [15]. Associated with the syndrome are also common reports of ruptures of the membranous labyrinth, usually involving Reissner's membrane, and the membranous duct walls of the utricle, saccule and ampullae. Other theories suggest that Meniere's disease can sometimes occur after middle ear infections, where a viral infection has permanently damaged the stereocilia (or hair cells) of the semi-circular canals or otolith organs [23]. The mechanical deflection of these hair cells is directly related to the neural response of the vestibular afferent nerve fibres [15].

Meniere's disease still seems to be presently unexplained [24]. It is also a syndrome whose symptoms often disappear with age, but this is not always the case.

Electrocochleography (ECOG) is used for the diagnosis of Meniere's disease. ECOG usually involves an electrode (consisting of a wick) being placed on the tympanic membrane. This active electrode is referenced to an electrode attached to the ipsilateral earlobe with a ground electrode placed on the forehead [30]. The ear is normally stimulated with alternating polarity acoustic clicks [30].

Referring to Fig. 1, the SP is known to be a "DC" response that, to a certain degree, represents the envelope of the stimulus [31]. An enhanced SP has been observed in patient's suffering from Meniere's disease [30]. AP is an AC response caused by the synchronous firing of thousands of auditory nerve fibres [30].

For diagnostic purposes, the summation potential (SP), action potential (AP) and SP/AP amplitude ratio are usually analysed [30]. The SP/AP amplitude ratio seems to be a more consistent measure of the response, which varies from 0.1 to 0.4 in normal subjects (mean value of 0.25) (the variability is often attributed to electrode placement).

III. Materials And Methods

A. Calculating Matrix element values

The matrix values (3)-(5) were calculated using human parameter values [1], [12], [15], [3]. A number of simplifying assumptions were made. Firstly, simplified expressions for the integrals given by (7)-(9) from the Rabbitt, Damiano, and Grant text [1] were used, namely $m_n \approx \frac{\rho}{A_n} l_n, c_n \approx \frac{8\pi\mu l_n}{A_n^2}$, and $k_n \approx \frac{8\pi\gamma h}{A_c^2}$, where A_C= cross-section area of cupula, and $h = 0.7\sqrt{A_c/\pi}$ (thickness of cupula). From the Wilson and Jones text [12], the average radius of the cross-section of the slender (non-utricle) segments of the semi-circular canals is r = 0.02 *cm.* From various sources [12], [15], the average radius of the cross-section of the utricle segments (UA and UP) was estimated to be approximately 3r. This allowed us to calculate the average cross-sectional area A_n for the slender segments (HC, AC, and PC) and the utricle segments (UA and UP). The lengths of each segment (l_n) were estimated from the same texts [12], [15].

Both λ_γ and λ_μ were set to 8π, because it is assumed that there is only simple diaphragm displacement, and that the canals are rotated only at low frequencies (allowing the assumption of simple Poiseulle flow within the canals) [1].

Not all segments contained a cupula (for example, the UP or CC segments), so the [K] matrix had a couple of elements set to zero ($k_{UP} = k_{CC} = 0$).

B. Simulating General Rotations

In order to calculate the integral given by (11), the geometry of the semi-circular canals needed to be simplified/idealized.

The horizontal canal (segments HC, UA and UP connected together) was assumed to be a perfectly circular loop of radius 0.65/2 cm, which is the average radius of a semi-circular canal [12]. The CC segment was approximated to be a short, straight segment, protruding out from the horizontal canal. The AC and PC segments were approximated to be two perfectly circular arcs of radius 0.65/2 cm [12].

In order to ensure that the resulting line integral given by (11) stayed simple, the three-canal system was made to be *symmetrical*, where the AC and PC segments had the same length, and the UA and UP segments had the same length. The line integral (11) could then be easily calculated using MATLAB's symbolic math package.

The origin of the vector coordinate system for vector quantities in (11) was placed (relative to the vestibular system) in such a way that it coincided with the tilt chair's pivot *point* in our laboratory experiments. The orientation of the coordinate system is such that the x-z plane is parallel to the *sagittal* plane of the human head (the plane that divides the human head into left and right parts). Both the anterior and posterior semi-circular canals are in vertical planes (perpendicular to the x-y plane), and they are oriented at an angle of 45 degrees to the sagittal plane [15]. The horizontal canal lies in the x-y plane. With the orientation of the coordinate system defined in such a way, $\vec{m} = i$ corresponds to an ipsi-lateral (sideways, to the left) rotation, $\vec{m} = j$ corresponds to a backwards rotation, and $\vec{m} = k$ corresponds to a horizontal rotation, where *i*, *j*, and *k* are unit vectors parallel to the x, y and z-axes, respectively.

The simulations of volume fluid displacements (described in the next section) were performed for the *left* ear. However, for any given $\vec{m}$, the volume fluid displacements in the right vestibular labyrinth can be deduced from the displacements in the left – they are simply the *negative* of waveforms calculated for the left vestibular labyrinth.

One limitation of the model is the simplified geometry (cross-sectional area A of the utricle and slender segments was kept constant in (7)-(9)). The line integral (11) was also simplified, neglecting the more complex shape of the canals. Further work could be done to take into account the more exact geometry of the canals, like the asymmetry of the vestibular labyrinth.

However, computer simulations that approximated an asymmetrical model of the vestibular labyrinth showed that it was only fluid flow in the posterior canal and the posterior section of the utricle that were affected (the amplitude of fluid flow was approximately halved there). The fluid flow in other parts of the vestibular labyrinth stayed the same. Therefore, based on these estimates, the simplified symmetrical model is a good approximation.

C. Solving for $\vec{Q}(t)$, α and u(t)

As shown by Rabbitt, Damiano and Grant [1], (1) can be recast as a symmetric system of six first order differential equations. This system of six equations can be expressed in the Laplace domain (the tilde above a certain quantity indicates that it is being expressed in the Laplace domain), and is given by

$$\tilde{\vec{Q}}^* = \tilde{s}\left\{[C^*]\tilde{s} + [K^*]\right\}^{-1}\tilde{\vec{G}}^* = [T]\tilde{\vec{G}}^*, \tag{18}$$

where

$$\vec{Q}^* = \begin{pmatrix} \dfrac{d\vec{Q}}{dt} \\ \vec{Q} \end{pmatrix}, \tag{19}$$

$$[C^*] = \begin{pmatrix} [0] & [M] \\ [M] & [C] \end{pmatrix}, \tag{20}$$

$$[K^*] = \begin{pmatrix} -[M] & [0] \\ [0] & [K] \end{pmatrix}, \tag{21}$$

$$[T] = \tilde{s}\left\{[C^*]\tilde{s} + [K^*]\right\}^{-1}, \tag{22}$$

$$\tilde{\vec{G}}^* = \dot{\tilde{\Omega}}\begin{pmatrix} \vec{0} \\ \vec{g} \end{pmatrix}, \tag{23}$$

and

$$\vec{g} = \begin{pmatrix} -g_{HC} - g_{UA} - g_{UP} \\ -g_{AC} - g_{CC} - g_{UA} \\ -g_{PC} - g_{CC} + g_{UP} \end{pmatrix}. \tag{24}$$

By taking the inverse Laplace transform of (18), we obtain $\vec{Q}^*$, where the last three elements of this vector contain the solution for $\vec{Q}(t)$. The Symbolic Math Package in MATLAB was used to find the inverse Laplace transform of (18), as well as computing the transfer matrix, [T].

The angular velocity applied to the canals (in the Laplace domain) is $\dot{\tilde{\Omega}}$, and appears in (23). In our laboratory experiments, the tilt chair applies a low frequency half-cycle sinusoid velocity (justifying $\lambda_\gamma = \lambda_\mu = 8\pi$) in order to rotate a patient. So, $\dot{\Omega}$ was set to equal a half cycle sinusoid, in order to correspond with the laboratory work. In the Laplace domain, this is expressed as

$$\dddot{\Omega} = A\left(\frac{\omega}{\omega^2 + s^2} + \frac{\omega}{\omega^2 + s^2} e^{-s\frac{\pi}{\omega}}\right), \quad (25)$$

where A is the amplitude, and ω the angular frequency.

When ω = 1, the half-cycle sinusoid has a width of π seconds. The rotations in our laboratory experiments last for approximately $3 \approx \pi$ seconds, so a half cycle sinusoid that lasts for π seconds corresponds to our laboratory experiments. The maximum angular velocity achieved in our laboratory is between 10 degrees/second and 15 degrees/second, so the amplitude, *A*, was set accordingly to simulate this.

The solution of the eigenvalue problem [1],

$$\left(\left([C^*]^{-1}[K^*]\right) + \alpha[I]\right)\vec{E} = \vec{0}, \quad (26)$$

provides six real valued time constants for the system, $\tau_n = 1/\alpha_n$, and the corresponding eigenvectors, $\vec{E}_n$ ([I] is the identity matrix). From the Kreyszig text [11], the six real valued constants, α_n, can be found by solving the equation

$$\det\left([C^*]^{-1}[K^*] + \alpha[I]\right) = 0. \quad (27)$$

The values of α that satisfy (27) are simply the eigenvalues [11] of the matrix $[C^*]^{-1}[K^*]$. In MATLAB, the function *eig(M)* finds the eigenvalues of any matrix, [M]. This MATLAB function was used to calculate the six constants, α_n.

In order the find the inverse Laplace transform of (15) in MATLAB, and solve for the gross displacement of the otolith layer, *u(t)*, an approximation of the component of gravity acting parallel to the otolith layer ($\vec{g}_{\parallel}$) needs to be made. The scalar expression for $\vec{g}_{\parallel}$ is given by $\left|\vec{g}_{\parallel}\right|$ = g $sin(\theta_U(t))$, where g = 980 cm s^{-2}, and $\theta_U(t)$ is the angle that the plane of the utricle makes with the horizontal plane at time *t* (seconds). We assume that the plane of the utricle is parallel with the (earth) horizontal plane before a tilt commences. In an ipsilateral tilt, the $\vec{g}_{\parallel}$ vector is in the lateral-anterior direction; in a backwards tilt, $\vec{g}_{\parallel}$ vector is in the posterior-lateral direction.

For an ipsilateral tilt (and also a backwards tilt), $\theta_U(t)$ is simply the integral of the angular velocity of the tilt chair (a half cycle sinusoid).

For small θ_U, $\sin(\theta_U) \approx \theta_U$. The angular position of the tilt chair (following an angular rotation) is still small enough for it to be approximated by $sin(\theta_U(t))$, and vice versa. So, we can say $\left|\vec{g}_{\parallel}\right|$ = g* $sin(\theta_U(t)) \approx$ g* $(\theta_U(t))$. This approximation allows us to find the inverse Laplace transform of (15) in MATLAB.

For angular velocities used in our laboratory experiments, a maximum error of 6% is introduced at the end of the time interval of rotation using such an approximation.

From Rabbitt et. al. [1], it is assumed that $5 < \tau_1 < 40\mu s$ and $0.1 < \tau_2 < 4\mu s$ in humans, based on data from Grant et. al. [32],[33]. In the simulations, τ_2 was given the value of 1.95 μs, and τ_1 was given a value 17.5 μs (the midpoints of the intervals for τ_2 and τ_1). However, both τ_2 and τ_1 were varied, to make sure that the general 'shape' of the utricular macula displacement stayed the same over the given intervals for τ_2 and τ_1.

Also, a plot of the utricular macula displacement using de Vries model [21] time constants of $\tau_2 \approx 2\times10^{-3}$ seconds, and $\tau_1 \approx 3\times10^{-2}$ seconds was done for comparison, even though these time constants have been criticized for being too large [19].

D. Simple Neural Model

The electrode in our laboratory experiments recorded field potentials from all three canals, utricle and saccule – the firing rate recorded was the sum of all these field potentials. In this section, a simple method for modeling the firing rate from both the canals and utricle will be shown.

The resting firing rate for an average canal afferent is taken to have a mean of 90 spikes/second [25]. The largest gains of canal afferents in the chinchilla are 2-3 spikes $\cdot s^{-1}$/deg $\cdot s^{-1}$ [25]. If we assume the regular units can fire at this maximum rate, then from the graph of logarithmic afferent gain for regular units in Goldberg et. al. [25], we have

$$0.094dB = 10\log\frac{3spikes \cdot s^{-1} / \deg \cdot s^{-1}}{G_0}, \quad (28)$$

where G_0 is the firing rate gain corresponding to *0 dB* (decibels). In our laboratory experiments, the half cycle sinusoid angular velocity has a frequency of ~ 0.167 Hz, which corresponds to the afferent gain of *0 dB* (decibels). So, the firing rate gain at 0.167 Hz is G_0 = 2.4 spikes $\cdot s^{-1}$/deg $\cdot s^{-1}$. This canal afferent gain is most likely overestimated, as the canal afferent gain for regular units was calculated to be 0.166 spikes $\cdot s^{-1}$/deg $\cdot s^{-1}$ at a 0.5 Hz head velocity in the macaque monkey [26].

The afferents innervating one of the semicircular canal crista will have a firing rate according to:

(Resting firing rate of average afferent + G_0*Peak Cupula Velocity*(Normalized Canal Firing Rate))× (Number of haircells on crista/Number of Hair cells per afferent), (29)

where the Peak Cupula Velocity is the maximum cupula velocity of the most stimulated canal for a given tilt, and the Normalized Canal Firing Rate is simply the fluid volume displacements (calculated by the inverse Laplace transform of

(18)) divided by the maximum fluid volume displacement of the most stimulated canal for a given tilt.

It can be shown that the total firing rate of the utricular macula (TotalFR) can be approximated by the product of the gross otolith layer displacement, *u(t)*, and the length of a Shear Sensitivity Vector [7] parallel to it. A polar diagram of 8 Shear Sensitivity Vectors is derived in work by Tribukait and Rosenhall [7]. The function *u(t)* can be found by taking the inverse Laplace transform of (15) in MATLAB.

The shear sensitivity vector that has the closest 'direction' to $\vec{u}$ at time *t* has its magnitude (or length) chosen to 'scale' *u(t)*, which is expressed as:

$$TotalFR \propto Scaled \cdot u(t) = u(t) \times \text{Magnitude of Shear Sensitivity Vector(t)}, \quad (30)$$

where the Magnitude of Shear Sensitivity Vector(t) is the length of the sensitivity vector chosen at time, t (seconds).

The scaled *u(t)* of (30) was then normalized, giving the 'largest' scaled *u(t)* value (from each of the three rotations – ipsilateral, backwards and horizontal) a value of 1.0.

The firing rate of a utricular afferent varies very approximately 'linearly' with $\boldsymbol{g}$ (gravity) applied parallel to the otolith membrane, in the 0 to 3$\boldsymbol{g}$ range [34].

For a cat [12], an average utricular afferent has a gain of 25 spikes/second per *g* (force of gravity), and similar gains are found in the chinchilla [19].

For an ipsilateral or backwards tilt, when the tilt chair is at a maximum angular displacement, 0.5$\boldsymbol{g}$ will be acting parallel to the otolith membrane – so, the average utricle afferent will be firing at $\approx 0.5\boldsymbol{g} \times 25$ spikes/second per $\boldsymbol{g}$ = 12.5 spikes/second above resting rate. If we multiply the normalized scaled u(t) curves by the Gain = 12.5 spikes/second, and add it to the resting rate, it will give us an 'estimate' of the firing rate (in spikes/second) of an average utricle afferent.

The normalized scaled *u(t)* curve that has a maximum value of 1.0 will get the full 12.5 spikes/second above resting rate value at its max. point; the other normalized scaled *u(t)* curves will be smaller (scaled down by the directional sensitivity). The firing rate of afferents innervating the utricular macula has the form of:

(Gain × normalized scaled *u(t)* + resting rate) × (Number of haircells on the utricular macula)/Number of Hair cells per afferent). (31)

The shape of this curve is determined mainly by the normalized scaled *u(t)* term. In the rodent species *Cavia*, the utricular macula had 9260 hair cells [27].

As dimorphic units tend to be the most common type of afferent fiber that innervate both the utricle and semicircular canal cristae [28], [25], we can make a simplifying assumption that only dimorphic units innervate the vestibular organ. The average dimorphic unit synapses with approximately 4-100 hair cells [25], or up to 130 hair cells for the utricle [28]. So, we can approximate that a dimorphic unit synapses with an average of 55 hair cells.

If we add (29) (for each canal) and (31) - this will give us the estimated *true* firing rate (the firing rate of all afferents innervating the vestibular organ - minus the saccule). This is done for the ipsilateral and contralateral tilt.

E. Electrovestibulography (EVestG) Recording Methods

The electrodes are attached to the subject, and record the vestibular signal. The recorded signals go to a PC either via a sound card or a data acquisition interface.

To avoid the non-linear frequency response of sound cards, a Cambridge biological pre-amplifier (CED 1902) was used, with the data then transferred into a CED 1401.

The most important aspect of an EvestG is that a head tilt is used as the drive stimulus in recordings. Using a vestibular stimulus (rather than, say, an auditory one) gives a more direct measure of vestibular activity.

As the electrode is placed to rest against the tympanic membrane, it is important to keep the subjects' movement after its insertion to a minimum. Subjects are asked to keep their eyes closed during recordings to reduce ocular artefacts.

The subject's ear canal is checked for cerumen (ear wax). The electrode is then secured to the patient with a piece of tape to stop the weight of the cable from pulling the electrode out of position.

The active electrode used for the recordings is a Bio-logic TM-EcochGtrode. It consists of a fine silver wire encased within a thin flexible tube. The tip features a soft, conductive hydrogel, which is moistened using conductive gel and saline, before it is placed inside the ear. This increases electrical contact with the tympanic membrane. The CED 1902 amplifier settings are controlled using Spike 2 installed on the PC. The gain of the amplifier is set so that the recorded signal does not saturate.

The head tilts are either voluntary or applied. Applied tilts are performed as there is a considerable amount of muscle activity in the former.

In applied head tilts, an hydraulic tilt chair is used. The hydraulic tilt chair is a cushioned chair on which the subject sits during the experiment. It is used as the stimulus to invoke the vestibular response that is recorded. The chair is computer controlled, to create body tilts as desired. These movements include tilting forward, back, left and right, rotation, up and down and also forward and back with the head rest. The room in which the experiments are performed is acoustically quiet and electrically isolated, which eliminates unwanted noise. The hydraulic tilt chair is controlled via computer using an assembler like language on a DMC Smart Terminal.

The tilts applied by the hydraulic tilt chair are half cycle sinusoidal rotations that last for 3 seconds (except in the up and down movements – which are linear accelerations in the up and down directions). The maximum angular velocity achieved in our laboratory experiments (in rotational movements, such as in ipsilateral/contralateral, backwards/forwards and horizontal rotations) is between 10 degrees/second and 15 degrees/second. So, there is a maximum error of 33% in the peak angular velocity. In the simulations, this will express itself only as an error in the amplitude of the curves (not in their shapes). This is because

the peak angular velocity is the constant, *A*, in (25), (23) and (18); when performing the inverse Laplace transform of (18), the constant *A* can be taken outside of the inverse Laplace transform operation, meaning that it will only have an effect on the amplitude but not the shape of the resulting fluid volume displacement and velocity curves.

The recorded signals are analysed using two different techniques. To observe the spectral response, the signals are wavelet decomposed. A Morlet wavelet was selected for its excellent time-frequency localisation property.

A devised neural event detection routine [20], [22] has also been used to extract vestibular neural events. The results obtained using this routine are similar to those used to extract the mentioned SP/AP ratio [29].

A typical vestibular recording (following a head tilt) is shown in Fig. 3.

The recording can be broken up into several stages: the onset stage (immediately following a tilt), an onset + transient stage, and then the steady state, as shown in Fig. 3.

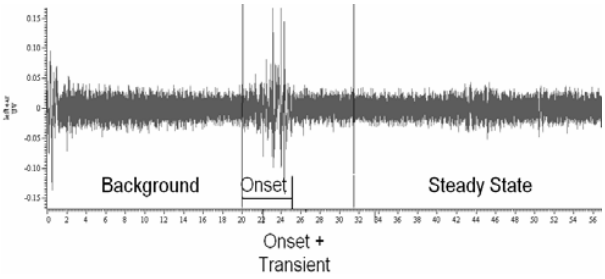

Fig. 3 Time segmentation of the raw recorded signal [35].

The background signal was recorded for 20 seconds with the patient in a tilt chair resting their head/neck against a neck rest. This segment represents the first t = 0-20 seconds. The patient was then tilted, reaching a maximum velocity of between 10 degrees/second and 15 degrees/second, coming to rest after 3 seconds. The onset (tilt) region was labeled at t= 20-25 seconds, onset + transient 20-30 seconds, steady state 30-40 seconds (refer to Fig. 3). The patient was then returned to an upright position over approximately 3 seconds. The up onset was labeled at t = 40-45 sec, up onset + transient 40-50 sec, up steady state 50-60 sec.

The patient is rotated in the tilt chair at the start of the *onset* phase in Fig. 3. The first 1.5 seconds of the onset phase is known as *onAA*, and *onBB* is the next 1.5 seconds.

IV. Neural Recording Results

Fig. 4 shows the smoothed averaged onAA, onBB and BGi (1.5 seconds of background recording immediately before onAA phase) responses for an ipsilateral tilt, results that were recently published in a paper by Lithgow and Heibert [35]. The BGi responses are most like a typical ECOG response displaying a well-defined Sp plateau [35]. The BGi plots show that the average Meniere's Sp/Ap ratio to be higher, as expected, than that for age matched Controls.

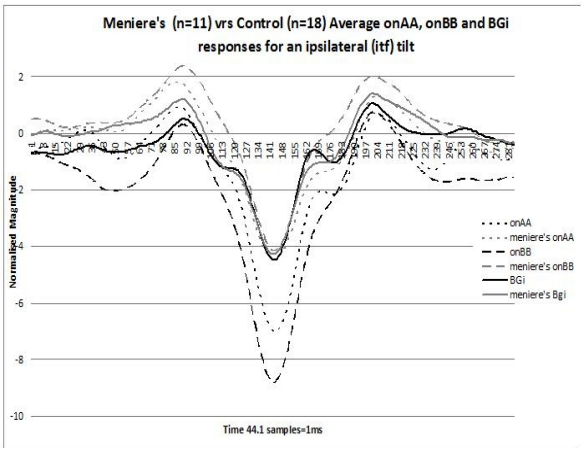

Fig. 4 The onAA, onBB and BGi (1.5 seconds of background recording before onAA) EVestG plots for an ipsilateral tilt [35].

The BGi responses are amplitude-wise smaller than either the onAA or onBB responses.

The Control (and to a lesser extent, the Meniere's group) BGi, onAA and onBB responses progressively increase in amplitude.

However, it can be seen that the Meniere's onBB response has an Ap amplitude almost *identical* to the Meniere's onAA Ap amplitude. On the other hand, the Ap amplitude of the Control onBB response is, in comparison, clearly larger than the Ap amplitude of the Control onAA response.

Fig. 5 shows the smoothed averaged BGi-onAA and BGi-onBB responses for an ipsilateral tilt, highlighting dynamic response changes in moving from a background to either an acceleration of deceleration phase [35]. The BGi-onAA (and BGi-onBB) responses were generated by subtracting the onAA plot from the BGi plot for each individual subject after normalizing each subject's responses by dividing by the largest of the measure "max value-min value" for either the BGi, onAA or onBB responses. These normalized plots were then averaged. The mean and standard deviation were generated for each point on the EVestG plot. The light shaded area in each plot shows regions where mean plus (or minus) the standard error (SE) is different for Controls and Meniere's groups. The dark shaded area is where a better than 90% confidence is obtained for plot loci differences between the Control and Meniere's groups. This provides some statistical validation of the differences between the two groups.

In the BGi-onAA plot, there is an apparent difference in the Ap tip region (sample numbers 135-160) appearing as a reduced Ap tip magnitude when moving from a BGi to an onAA response (Fig. 5) for Meniere's patients.

In the BGi-onBB plot there is an apparent difference that almost the entire plot is being upwardly offset for Meniere's versus Control subjects.

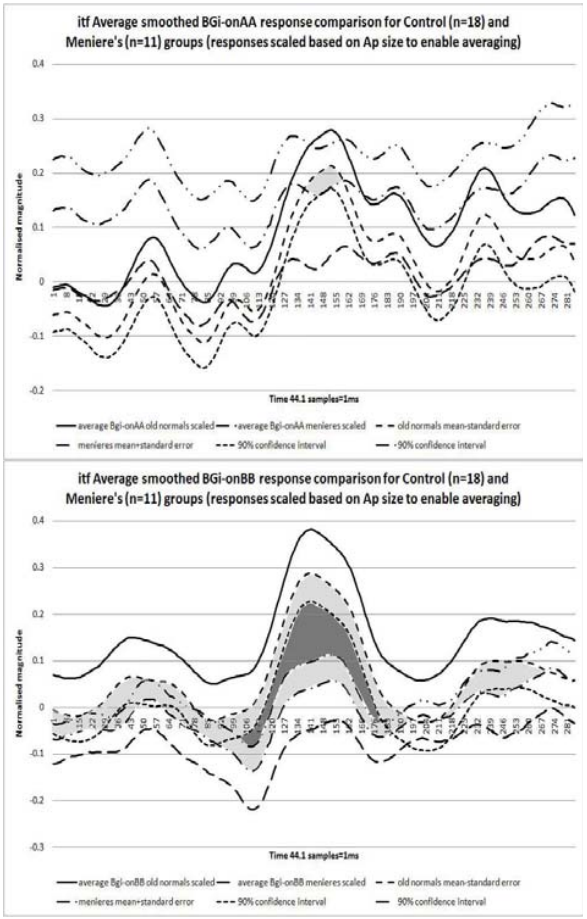

Fig. 5 BGi – onAA (top) and BGi – onBB (bottom) responses [35].

The averaged onAA, onBB and BGi responses for a contralateral tilt are almost identical to those for an ipsilateral tilt in Fig. 4.

V. Simulation Results

The simulation results were checked for their correctness by making sure all the volume fluid displacement curves plotted satisfied (12) to (14), which they did.

A. Sensitivity of Results to Parameter Changes

For any computer model of a biological system, parameters that characterize the system can only be specified with a limited accuracy. In this model, a number of approximations have been made, therefore it is expected that some errors have been introduced into the results.

Using (27), the dominant time constant for all these plots was calculated to be approximately 10 seconds, which is close to the experimental value of 13 seconds [1], [12]. This shows that the simulation time constants correspond to the experimental observation within about 30%.

The various model parameters (μ, γ, ρ, r, and Utricle radius) were varied, to see how sensitive the system is to parameter changes. It was found that the 'general' shape of the volume fluid displacement curves in each part of the vestibular labyrinth (as shown in Fig. 6) did not change for a fairly broad range of parameter values. The model was tested over the following *normalized* parameter ranges: $0.1 < \mu^* < 1.5$, $0.1 < \gamma^* < 2.5$, $0.7 < \rho^* < 1.2$, $0.7 < r^* < 2.0$, $0.3 <$ Ampulla radius* < 3.0 and $0.3 <$ Utricle radius* < 3.0 (where an asterisk denotes that the parameter has been normalized). The parameters were normalized by dividing them by the normal (healthy) parameter values. Although the healthy (normal) parameter values are to be viewed with caution with regards to their accuracy, it can be expected that they will fall within the ranges given above [1], [16]. Therefore, we can be confident that the general shape of the curves is accurate.

In Fig. 6, two important points on the general fluid volume displacement curve were monitored as the parameter values were varied: the peak fluid volume displacement, and peak *rebound* fluid volume displacement.

The peak *rebound* fluid volume displacement was identified by Obrist [17] as being the so-called 'velocity error'. It was speculated by Obrist [17], [39] that if the velocity error is strong enough, it could lead to a sensation of *reverse* angular motion (and thus, balance problems).

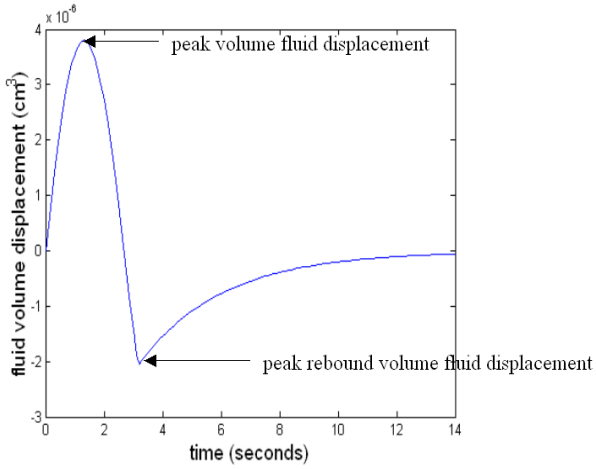

Fig. 6 The peak volume fluid displacement, and peak *rebound* volume fluid displacement shown on a typical fluid volume displacement curve.

Interestingly, in the simulation of hydrops (increased fluid volume) in the ampullae, the peak rebound fluid volume displacement was strongly attenuated, even for small cases of hydrops (and for all head tilts). For Ampulla radius* = 3.0, the peak rebound fluid volume displacement was reduced by 93% in the most stimulated canal, and to an even greater extent in the other (less stimulated) canals. This is an interesting finding, as hydrops in the ampullae and utricle has been associated with Meniere's Disease in some cases [40].

B. Utricle Response Results

The simulation of the mechanical utricular macula response shows that gravity dominates the response during ipsilateral/backwards tilts.

The maximum displacement of the utricular macula due to gravity is nearly 5 orders of magnitude larger than its displacement due to fluid flow in an ipsilateral tilt (the same is true in a back tilt). Indeed, the displacement due to gravity so many times larger in magnitude than the displacement due to fluid flow for both tilts, that fluid flow does not affect the overall shape of the utricular macula displacement curves at all.

These modeling results support the notion that the utricular macula is primarily a gravity/linear acceleration sensor, as the lateral vestibular nucleus (innervated by the utricle and saccule) transmits signals to the spinal cord through the lateral vestibulospinal tract; static movement is controlled by these signals [27]. Indeed, static movements are largely responses to gravity [27].

In these simulations, the midpoints of the intervals $5 < \tau_1 < 40 \mu s$ and $0.1 < \tau_2 < 4 \mu s$ were used as the two otolith time constant values. The values of the time constants were also varied. It was found that the general shape of the curves stayed the same, although the mechanical displacement of the utricular macula was larger for longer time constants (at the upper ends of the intervals $5 < \tau_1 < 40 \mu s$ and $0.1 < \tau_2 < 4 \mu s$).

Finally, a simulation was performed using the time constants predicted by the De Vries model [19]. The general shape of the curves remained the same; again, the shape of the curves during ipsilateral/backwards tilts is dominated by the effects of gravity parallel to the plane of the utricle (as a function of time). The mechanical displacement is 6 orders of magnitude larger using the De Vries model time constants, compared to the displacements using the Grant and Best time constants [1], [32].

The utricular afferent firing rate curves (see the following section for more details) using the De Vries model time constants have the same shape/relative amplitudes as the ones using the Grant and Best time constants. So, despite the De Vries time constants being criticized for causing the model to have a too high mechanical sensitivity [19], the firing rates they predict are almost identical to the rates calculated using time constants τ_1 = 17.5 μs and τ_2 =1.95 μs .

C. Neural Modeling Results

As described in the simple neural model, the afferents innervating one of the semicircular canals will have a firing rate according to (29). For an ipsilateral tilt, the firing rates of the three canals are plotted in Fig. 7.

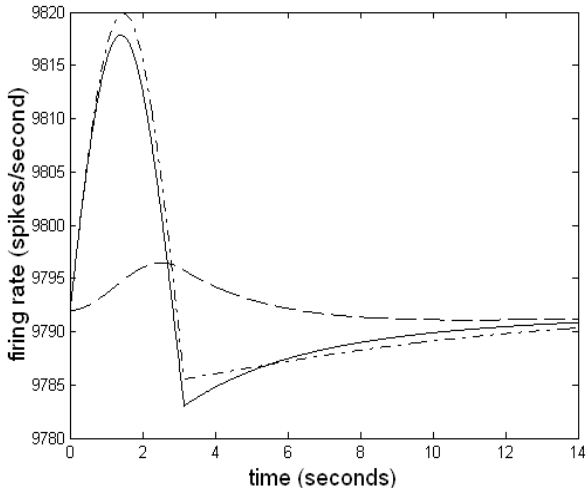

Fig. 7 The simulated semicircular canal firing rates (in spikes/second), for the anterior canal (solid line), horizontal canal (dashed line) and posterior canal (dash dotted) during an ipsilateral tilt.

Likewise, the firing rate of the afferents innervating the utricular macula is given by (31). For an ipsilateral tilt, the firing rate of the utricular macula is given by Fig. 8.

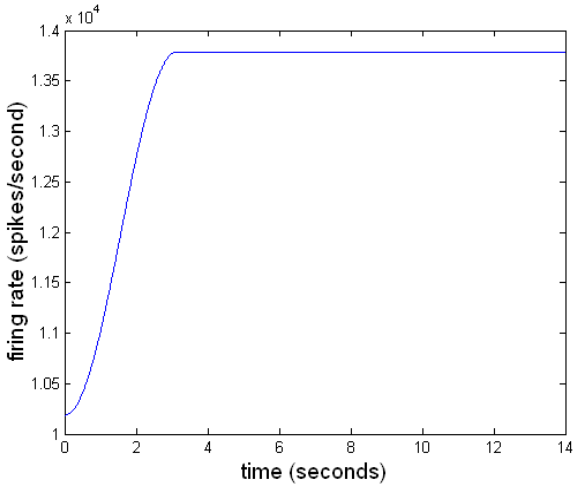

Fig. 8 The simulated firing rate (in spikes/second) of utricular afferents, during an ipsilateral tilt

The electrode in our laboratory experiments will record firing rates from all three canals, and the utricle – this firing rate will be the sum of all three canal firing rates in Fig. 7, plus the firing rate of utricular afferents in Fig. 8. This sum is plotted in Fig. 9.

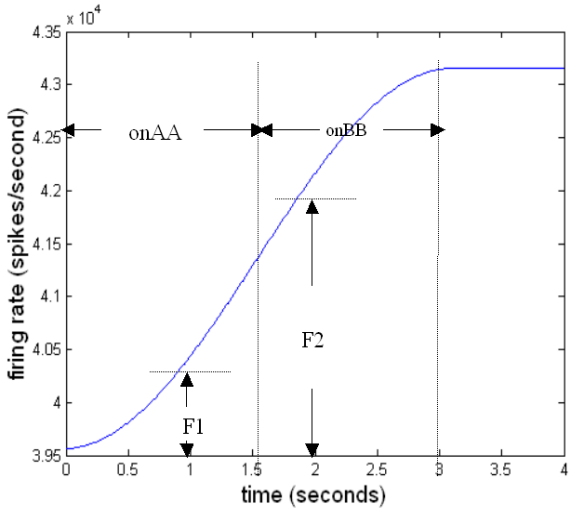

Fig. 9 The simulation of the 'total' firing rate of both canal and utricle afferents, where F1 is the average firing rate in the onAA phase, and F2 is the average firing rate in the onBB phase.

Fig. 9 shows the total firing rate of all canal and utricular afferents during an ipsilateral tilt, with the onAA and onBB phases shown. The shape of the curve is dominated by the utricle response.

If it is assumed that neural activity of the saccule and efferent fibers is negligible (which may be a reasonable assumption, as the electrical potential of the utricle has a greater dynamic range than that of the saccule [36]), then we can expect the simulated firing rate in Fig. 9 to dominate the EVestG recordings. To test this hypothesis, we calculate the average firing rates in the onBB and onAA phases of Fig. 9, and compare it to the Ap amplitudes of the EVestG plot for an ipsilateral tilt in Fig. 4.

The Ap amplitude of an EVestG plot is the average Ap amplitude of a number of test subject recordings for a particular time segment – therefore, the average firing rate in a given time segment should be proportional to the corresponding EVestG plot's Ap amplitude (assuming there were no unusually large or small individual subject responses dominating the averaged response in Fig. 4, which there weren't – normalization of individual subject plots prior to summing and averaging could solve such a potential problem in future work). In Fig. 9, F1 is the average firing rate in the onAA phase, and F2 is the average firing rate in the onBB phase. Likewise, we define AP1 as the AP amplitude in the onAA phase, and AP2 the AP amplitude in the onBB phase. We hypothesize that $F1 \propto AP1$, and $F2 \propto AP2$.

From Fig. 9, F2/F1 = 1.06 (3 significant figures) ≈ 1.1 (2 significant figures). So, the firing rate increases by 6% when going from the onAA phase to the onBB phase, using 3 significant figures; the firing rate increases by 10% when using 2 significant figures. Because one of the model parameters used in creating the simulations is specified with an accuracy of only 2 significant figures, it is appropriate to round off the F2/F1 ratio to 2 significant figures.

The curve in Fig. 9 was plotted assuming that the laboratory tilt chair had a maximum angular velocity of 15 degrees/second. The maximum angular velocity is between 10 degrees/second and 15 degrees/second. Using the lower peak angular velocity of 10 degrees/second, F2/F1 = 1.04 (3 significant figures) i.e. a 4% firing rate increase when going from onAA to onBB.

The AP amplitude is measured as the magnitude of the difference between the SP point and the AP point, as shown in Fig. 1. In Fig. 4, the SP point (for normals) is -1.5 ± 0.2 SE (Standard Error). The AP point for normals in the onAA phase and onBB phase is -7.0 ± 0.2 SE and -8.8 ± 0.25 SE respectively. Neglecting the standard errors, AP2/AP1 = (8.8 – 1.5)/(7.0-1.5) = 7.3/5.5 = 1.33 i.e. there is a (mean) 33% change in the AP amplitude when moving from the onAA phase to the onBB phase. If the AP amplitude is taken as a measure of the firing rate, then we can also say there is a 33% change in firing rate when going from onAA to onBB during an ipsilateral tilt.

Taking into account the standard errors, AP2/AP1 = $\frac{7.3 \pm 0.33}{5.5 \pm 0.29} = 1.33 \pm 0.067$ SE, where the standard errors of differences and quotients were calculated using the E.C. Fieler method [37]. The 95% confidence interval for the ipsilateral AP2/AP1 ratio is given by $1.16 \le AP2/AP1 \le 1.53$; the 99% confidence interval is given by $1.10 \le AP2/AP1 \le 1.61$. We notice that the F2/F1 ratio calculated for the ipsilateral head tilt response in Fig. 9 is 1.1 (using 2 significant figures, and assuming peak angular velocity of 15 degrees/second), which fits into the lower end of the 99% confidence interval for AP2/AP1. So, there is some congruence here with the notion that $F1 \propto AP1$, and $F2 \propto AP2$.

The simulation of the total firing rate for a contralateral tilt produced a curve identical to the one in Fig. 9, with F2/F1 = 1.1 (2 significant figures, assuming peak angular velocity of 15 degrees/second) - the same as in an ipsilateral tilt. Likewise, for a backwards tilt, F2/F1 = 1.07 (3 significant figures), which is slightly higher than F2/F1 = 1.06 (3 significant figures) for an ipsilateral tilt. This was expected, as the normalized firing rates showed that backwards tilt produces the highest firing rate in the utricle.

The shape of both curves (for contralateral and back tilt responses) is dominated by the utricle response, as in Fig. 9.

VI. Discussion

A. Neural Simulation Results

The simulations of the 'true' firing rate of all utricular and canal afferents was made, using experimental data based on rodents [27]. In Fig. 9, F2/F1 = 1.1, where F1 is the average firing rate in the onAA phase, and F2 is the average firing rate in the onBB phase. AP2/AP1 = 1.33 ± 0.067 (Standard

error), where AP1 is the AP amplitude in the onAA phase, and AP2 is the AP amplitude in the onBB phase in the EVestG plot for an ipsilateral tilt (see Fig. 4). The ipsilateral F2/F1 ratio is 1.1, which fits into the lower end of the 99% confidence interval for AP2/AP1. So, there is some congruence with the notion that perhaps $F1 \propto AP1$, and $F2 \propto AP2$, and that the utricle response dominates the EVestG recordings (as the firing rate in Fig. 9 is dominated by the utricle response). However, it is also possible that the neural activity from the saccule and the efferent fibers contribute non-trivially to the EVestG recordings, which may account for the fact why F2/F1 = 1.1 < AP2/AP1 = 1.33 (its mean value).

Interestingly, the 'true' firing rate of all utricular and canal afferents during a contralateral tilt is the same as that for an ipsilateral tilt, as shown in Fig. 9. The EVestG plot for a contralateral tilt shows an Ap amplitude larger in the onBB phase than it is in the onAA phase - much the same as in the EVestG plot for an ipsilateral tilt in Fig. 4.

So, the notion that the firing rate of the utricle dominates the EVestG recordings provides a good explanation for the Ap amplitudes of EVestG plots for both ipsilateral and contralateral tilts.

A dominant utricular firing rate can potentially contain diagnostic information about hair cell damage. It is expected that hair cell damage in the utricle would result in a decreased dynamic response, which is interestingly what the EVestG plot in Fig. 4 indicates for Meniere's patients.

In the simulation results, it was found that the peak rebound fluid volume displacement (see Fig. 6) in the canals was strongly attenuated when the fluid volume increased in the ampullae (for all head tilts). Such excess fluid in the ampullae has been associated with Meniere's Disease [40]. Therefore, an attenuated peak rebound fluid volume displacement in the canals could provide diagnostic information about hydrops (excess fluid volume) in the vestibular labyrinth. However, with the simple neural modeling results predicting that the utricular firing rate will dominate the EVestG recordings, any diagnostic information in the canal firing rates will be overpowered by the utricle response. Further signal processing work would need to be done in order to extract the canal firing rates.

B. Model Limitations

The modeling results based on the three-canal model have a number of significant limitations. Firstly, the geometry of the vestibular labyrinth was significantly idealized – it essentially captured only the 'gross' circular shape of the canals, and the average diameters of the ampulla, utricle and slender segments of the canal. Ideally, it would be best to use histological data based on a real human vestibular labyrinth, as was used in modeling by Rajguru et. al. [16].

The model of 'gross' displacement of the utricular macula [1] has its limitations, as it does not take into account the three-dimensional curvature of the macula [34], [38], essentially treating it as a flat, two-dimensional membrane. Furthermore, the macro-mechanical model of the utricle allows only a calculation of its 'average' displacement, unlike the finite element model of Jaeger et. al. [34], where different parts of the macula can have different displacements.

However, in defence of the macro-mechanical model of the utricle, the Jaeger et. al. model showed that the utricular macula has a small enough elasticity to allow each small part of the macula to act 'independently' of all other parts [34]. In a sense, the macula can be divided into a large number of independent 'linear acceleration sensors', with each one most sensitive to a particular direction of linear acceleration (based on its local orientation in space, which is largely horizontal, or up to a 30 degrees angle to the earth's horizontal [38] when the head is in an upright position). So, in the presence of gravity, it is expected that each 'part' of the macula will have a displacement in the direction of gravity, much like the macro-mechanical model [1]. Its directional sensitivity will be a little different from the two-dimensional directional sensitivity calculated by Rosenhall [7], as the Jaeger et. al. model [34] takes in to account the three-dimensional curvature of the macula macula – but it should be somewhat similar, as the three-dimensional macula is still somewhat reasonably flat [38].

Therefore, the simple macro-mechanical model [1] still can provide some insight into the biomechanics of the utricular macula. A limitation of the simple neural model is that it assumes all the afferent fibers innervating the utricle and semi-circular canals are the same, which is not the case. However, the literature suggests that dimorphic units tend to predominate the fibers that innervate the vestibular system, with dimorphic units outnumbering calyx units by 3:1 in the utricle [28], meaning that treating all the afferents innervating the vestibular system as being the same is a good approximation.

VII. Conclusion

A number of main conclusions can be made from the results obtained:

- In the EVestG plot of Fig. 4, the BGi responses are most like a typical ECOG response displaying a well-defined Sp plateau [35]. The BGi plots show that the average Meniere's Sp/Ap ratio to be higher, as expected, than that for age matched Controls.
- For a broad range of parameter values, the three canal model [1] is ***stable,*** with the 'general shape' of the fluid volume displacement curves staying the same.
- The modeling results suggest that during the first 3 seconds of the onset phase (when a half cycle sinusoid angular velocity is applied to a subject), the fluid volume displacements within the vestibular labyrinth are half cycle sinusoids, followed by a period of exponential decay after the tilt has ceased; i.e., the canals are transducers of angular velocity applied to the head, disturbed

only by a so-called 'velocity error', first identified by Obrist [17]

- The modeling results strongly reinforce the notion that the utricular macula is mainly a gravity/linear acceleration sensor; during an ipsilateral/back tilt, the displacement due to gravity is 5 orders of magnitude larger than displacement due to endolymph flowing through the utricle - making the effect of fluid flow on the macula insignificant
- The modeling results (which don't take into account the neural responses of the saccule and efferent fibers) suggest that the EVestG recordings might be dominated by the utricle response in ipsilateral, contralateral and backward tilts. Indeed, the Ap amplitude of the EVestG plot for an ipsilateral tilt in the onBB phase (denoted by AP2) is 1.33 $(\pm 0.067 SE)$ times larger than that of the Ap amplitude in the onAA phase (denoted by AP1) i.e. AP2/AP1 = 1.33 ± 0.067 SE. The average firing rate of the all the canal and utricular afferents during an ipsilateral tilt in the onBB phase (denoted by F2) is 1.1 times larger than that of the average firing rate in the onAA phase (denoted by F1) i.e. F2/F1 = 1.1 (see Fig. 9). The ratio F2/F1 = 1.1 fits into the lower end of the 99% confidence interval for AP2/AP1, given by $1.10 \le AP2/AP1 \le 1.61$. So, there is some congruence with the notion that $F1 \propto AP1$, and $F2 \propto AP2$, and that the utricle response dominates the ipsilateral EVestG recordings (as the shape of the firing rate in Fig. 9 is dominated by the utricle response). Similar results are expected to be obtained for a contralateral tilt.
- A dominant utricular firing rate in an ipsilateral/backwards tilt can potentially contain diagnostic information about utricular hair cell damage caused by a viral infection (when using a half cycle sinusoid input velocity).

From these conclusions, we can make the following recommendations regarding future work and future areas of research:

- Ideally, it would be best to combine the finite element model of the utricular macula by Jaeger et. al. [34], together with a model that takes into account the multi-dimensional fluid flow in the ampulla, as in the Rabbitt and Damiano model [2]. The Rabbitt and Damiano [2] model would have to be extended, to include the transient responses.
- However, the suggestion above may in fact be unnecessarily complex, as very likely the effects of gravity will overpower the effects of fluid flow in the utricle when using the Jaeger et. al. model as well (as was shown in modeling results of this paper). The existing data from the Jaeger et. al. model [34] adequately take into account the curvature of the utricular macula, and how the local curvature responds to gravitational/linear acceleration applied to it.
- Ideally, it would be better to use histological data, as used in modeling of BPPV [16], that describes the geometry of the human semicircular canals and utricle- rather than the idealized geometry used in this paper.
- The effect of the saccule (not included in the modeling work presented here) on EVestG recordings should also be examined in the future; however, it is expected that the effect of the saccule will be negligible, as the electrical potential of the utricle has a greater dynamic range than that of the saccule [36].

ACKNOWLEDGMENT

Thanks to Neural Diagnostics Pty. Ltd. for support in this project.

REFERENCES

[1] Rabbitt R.D., Damiano E.R., and Grant J.W (2004), "Biomechanics of the Semicircular Canals and Otolith Organs", in The Vestibular System, Springer, Chapter 4.
[2] Damiano E.R. and Rabbitt R.D. (1996), "A Singular Perturbation Model of Fluid Dynamics in the Vestibular Semicircular Canal and Ampulla", The Journal of Fluid Mechanics, vol. 307, pp. 333-372.
[3] Rabbitt R.D. and Damiano E.R. (1992), "A hydro elastic model of macro mechanics in the endolymphatic vestibular canal", The Journal of Fluid Mechanics, vol. 238, pp. 337-369
[4] Aso S., Wattanabe Y., and Mizukoshi K. (1991), "A clinical study of electrocochleography in Meniere's disease", Acta. Otolaryngol. (Stockh.), vol. 111, pp. 44 – 52.
[5] Yamauchi A., Rabbitt R.D., Boyle R., and Highstein S.M. (2001), "Relationship between Inner-Ear Fluid Pressure and Semicircular Canal Afferent Nerve Discharge", The Journal of the Association for Research in Otolaryngology, vol. 03, pp. 26 - 44.
[6] Gibson W.P.R. and Prasher D.K. (1983), "Electrocochleography and its role in the diagnosis and monitoring of endolymphatic hydrops", Otolaryngol. Clin. North Am., vol. 16, pp. 59 – 68.
[7] Tribukait A. and Rosenhall U. (2001), "Directional Sensitivity of the Human Macula utriculi Based on Morphological Characteristics", The Journal of Audiology & Neuro-otology, vol. 6, pp. 98 – 107.
[8] Mosicki E. K., Elkins E.F., Baum H.M., and McNamara P.M. (1985), "Hearing loss in the elderly: an epidemiologic study of the Framingham Heart Study Cohort", Ear and Hearing, vol. 6(4), pp. 90 -184.
[9] Rabbitt R.D. and Highstein S.M. (1999), "Influence of Surgical Plugging on Horizontal Semicircular Canal Mechanics and Afferent Response Dynamics", The Journal of Neurophysiology, vol. 82, pp.1033-1052.
[10] Kim. H. H., Kumar. A., Battista R. A. and R. J. Wiet. (2005), "Electrocochleography in patients with Meniere's disease", American Journal of Otolaryngology, vol. 26, Issue 2 (March-April), pp. 128-131.
[11] Kreyszig E. (1993), Advanced Engineering Mathematics, Seventh Edition, John Wiley and Sons.
[12] Wilson V.J. and Jones G.M. (1979), Mammalian Vestibular Physiology, Plenum Press, New York.
[13] Shoushtarian M. (2005), The relationship between Electrovestibulography (EvestG) and Parkinson's Disease, Electrical and Computer Systems Engineering, Monash University (transfer report).
[14] Garrett, A. (2006), Characterisation of Sensory Cells within the Vestibular System Using Electrovestibulography (EVestG), Electrical and Computer Systems Engineering, Monash University (transfer report).

[15] Baloh R.W. and Honrubia V. (2001), Clinical Neurophysiology of the Vestibular System, Third Edition, Oxford University Press.
[16] Rajguru S.M., Ifediba M.A., and Rabbitt R.D. (2004), "Three-Dimensional Biomechanical Model of Benign Paroxysmal Positional Vertigo", Annals of Biomedical Engineering, vol. 32, no. 6, pp. 831 – 846.
[17] Obrist D. (2007), Fluid Mechanics of Semicircular Canals –Revisited, Institute Of Fluid Dynamics, ETH ZURICH, Sonneggstrasse 3, 8092 Zurich, Switzerland
[18] Lithgow B.J., Shoushtarian M., and Heibert D. (2006), "ElectroVestibuloGram (EVestG): The separation of Benign Paroxysmal Positional Vertigo and Meniere's Disease", MedSip2006, Glasgow, UK, CD Rom, 4 pages.
[19] Goldberg J.M. et al (1990), "The Vestibular Nerve of the Chinchilla IV. Discharge Properties of Utricular Afferents", The Journal of Neurophysiology, vol. 63, no. 4, pp. 781 –789.
[20] Lithgow B.J. (Inventor), "A neural event process", Patent, (WO2006/024102, priority date 1st September 2004).
[21] De Vries, H. (1950), "The mechanics of the labyrinth otoliths", Acta Oto-Laryngol., vol. 38, pp. 262 – 273.
[22] Lithgow B.J. (Inventor), "A neural event system", Patent, (PCT/AU2007/902924, priority date June 2007).
[23] Selmani Z., Marttila T., and Pyykko H. (2005), "Incidence of virus infection as a cause of Meniere's disease or endolymphatic hydrops assessed by electrocochleography", Eur. Arch. Otorhinolaryngol., vol. 262, pp. 331 – 334.
[24] Beasley B.J.P. and Jones N.S., (1996),"Historical Article- Meniere's Disease: evolution of a definition" The Journal of Laryngology and Otology, vol. 10, pp. 1107-1113.
[25] Lsyakowski A. and Goldberg J.M. (2004), "Morphophysiology of the Vestibular Periphery", in The Vestibular System, Springer, Chapter 3.
[26] Sadeghi S.G., Minor L.B., and Cullen K.E. (2007), "Response of Vestibular-Nerve Afferents to Active and Passive Rotations Under Normal Conditions and After Unilateral Labyrinthectomy", Journal of Neurophysiology, vol. 97, pp. 1503 – 1514.
[27] Lindenlaub T. et. al. (1995), "Convergent Evolution of the Vestibular Organ in the Subterranean Mole-Rats, Cryptomys and Spalax, as Compared With the Aboveground Rat, Rattus", Journal of Morphology, vol. 224, pp. 303-311.
[28] Goldberg J.M. et al (1990), "The Vestibular Nerve of the Chinchilla. V. Relation Between Afferent Discharge Properties and Peripheral Innervation Patterns in the Utricular Macula", Journal of Neurophysiology, vol. 63, no. 4, pp. 791 –804.
[29] Franz, B. (2002), "A method of measuring the activity of a biological system", Patent, International publication number WO 02/47547 A1.
[30] Ferraro J., Best L., and Kaufman I. (1983), "The use of electrocochleography in the diagnosis, assessment and monitoring of endolymphatic hydrops", Otolaryngologic clinics of North America, vol. 16, pp. 69-82.
[31] Dallos P. (1973), The auditory periphery: Biophysics and physiology, New York Academic Press.
[32] Grant J.W. and Cotton J.R. (1991), "A model for otolith dynamic response with viscoelastic gel layer", Journal of Vestibular Research, vol. 1, pp. 139 – 151.
[33] Grant J.W., Huang C.C. and Cotton J.R. (1994), "Theoretical mechanical frequency response of the otolithic organs", Journal of Vestibular Research, vol. 4, pp. 137 - 151.
[34] Jaeger R., Takagi A., and Haslwanter T. (2002), "Modeling the relation between head orientations and otolith responses in humans", Hearing Research, vol. 173, pp. 29 – 42.
[35] Lithgow B.J., Garrett A., and Heibert D. (2008), "EVestG: A Measure for Meniere's Disease", 29th Annual International Conference of the IEEE EMBS, Vancouver, Canada, 4 pages accepted.
[36] Smith C.A. et al (1958), "DC Potentials of the Membranous Labyrinth", Am. Journal of Physiology, vol. 193(I), pp. 203 – 206.
[37] Motulsky H. (1995), Intuitive Biostatistics, Oxford University Press, New York, pp. 285 – 286.
[38] Naganuma H. et al. (2003), "Three Dimensional Analysis of Morphological Aspects of the Human Utricular Macula", Ann. Otol. Rhinol. Laryngol., vol. 112, no. 5, pp. 419.
[39] Obrist D. and Hegemann S. (2007), Fluid Mechanics of Benign Paroxysmal Vertigo (BPPV), Institute Of Fluid Dynamics, ETH ZURICH, Sonneggstrasse 3, 8092 Zurich, Switzerland
[40] Hall J.W. (1992), Handbook of Auditory Evoked Responses, Allyn and Bacon; Needham Heights, Massachusetts.